Mesenchymal Stem Cells Shed Amphiregulin at the Surface of Lung Carcinoma Cells in a Juxtacrine Manner[1,2]

Oriane Carnet[*,3], Julie Lecomte[*,3], Anne Masset[*], Irina Primac[*], Tania Durré[*], Ludovic Maertens[*], Benoit Detry[*], Silvia Blacher[*], Christine Gilles[*], Christel Péqueux[*], Jenny Paupert[*], Jean-Michel Foidart[*], Guy Jerusalem[†], Didier Cataldo[*] and Agnès Noel[*]

*Laboratory of Tumor and Developmental Biology, GIGA-Cancer, University of Liège, B-4000 Liège, Belgium;
†Department of Medical Oncology, Centre Hospitalier Universitaire (CHU), Sart Tilman, B-4000 Liège, Belgium

Abstract

Solid tumors comprise cancer cells and different supportive stromal cells, including mesenchymal stem cells (MSCs), which have recently been shown to enhance tumor growth and metastasis. We provide new mechanistic insights into how bone marrow (BM)–derived MSCs co-injected with Lewis lung carcinoma cells promote tumor growth and metastasis in mice. The proinvasive effect of BM-MSCs exerted on tumor cells relies on an unprecedented juxtacrine action of BM-MSC, leading to the *trans*-shedding of amphiregulin (AREG) from the tumor cell membrane by tumor necrosis factor-α–converting enzyme carried by the BM-MSC plasma membrane. The released soluble AREG activates cancer cells and promotes their invasiveness. This novel concept is supported by the exploitation of different 2D and 3D culture systems and by pharmacological approaches using a tumor necrosis factor-α–converting enzyme inhibitor and AREG-blocking antibodies. Altogether, we here assign a new function to BM-MSC in tumor progression and establish an uncovered link between AREG and BM-MSC.

Neoplasia (2015) 17, 552–563

Introduction

Cancers have long been considered the consequence of DNA mutations, particularly in oncogenes and tumor-suppressive genes that affect cell proliferation and survival [1,2]. However, these cancer cell– and genome-centered models have overlooked the complex nature of the tumoral tissue. Indeed, cancer cells are embedded in a tumor stroma composed of extracellular matrix and stromal cells, such as endothelial and lymphatic cells, immune and inflammatory cells, and (myo)fibroblasts [3]. The complex cross talk between tumor and stromal cells influences tumor cell behavior and facilitates metastatic dissemination to distant organs [1,4–7]. Cancer cells themselves are also able to alter the adjacent tissue to establish a permissive and supportive environment for tumor progression [3].

Fibroblastic-like cells can be derived from the activation of resident cells or the recruitment of bone marrow (BM)–derived mesenchymal stem cells (MSCs) [7,8]. MSCs are now recognized as an important source of carcinoma-associated fibroblasts (CAFs) [4]. MSCs are multipotent progenitor cells characterized by their capacity for self-renewal and differentiation into chondrocytes, osteocytes, adipocytes, fibroblasts, and other cell types [5,9]. Growing evidence has shown the crucial contribution of MSCs to malignant progression.

Depending on the system used, MSCs have been shown to favor tumor growth and cancer metastasis by promoting angiogenesis, increasing the invasive properties of tumor cells, or preventing tumor cell recognition by the immune system [6,10–12]. On the other hand, few studies have

suggested an inhibitory effect of MSCs on tumor progression [13,14]. The cross talk between cancer cells and MSCs occurs mainly through paracrine signaling mechanisms that are mediated by the secretion of soluble factors, including cytokines, chemokines, growth factors, and proteases [6,12,15–17]. Among these factors, the epidermal growth factor receptor (EGFR) ligand family plays a crucial role.

Amphiregulin (AREG) is one of the seven members of the EGFR ligand family (including HB-EGF, EGF, betacellulin, TGF-alpha, neuregulin, and epiregulin). AREG interacts exclusively with EGFR (also named HER1 or c-Erb1) but with less affinity than EGF and activates subsequent signaling pathways such as MAPK, PI3/Akt, and STAT3. AREG is expressed as a transmembrane precursor, which is activated through a proteolytic cleavage that involves tumor necrosis factor-α–converting enzyme (TACE), which is also referred to as ADAM17 [18] and is a transmembrane protease implicated in the shedding of many substrates [19]. This shedding gives rise to various forms of AREG, either secreted or membrane bound, which act in an autocrine, paracrine, or juxtacrine manner on cells in the direct neighborhood or at distant sites [20,21]. Several studies report protumoral and proinflammatory roles of TACE [22].

In this study, we found that juxtacrine-mediated interactions between BM-MSCs and Lewis lung carcinoma (LLC) cells stimulate the *in vivo* and *in vitro* proliferative and invasive properties of cancer cells. BM-MSCs shed AREG from cancer cell membrane through TACE activity, as assessed by a pharmacological approach. The functional implication of AREG in cancer cell invasion is supported by its inhibition with AREG-blocking antibodies. We are thus assigning a novel function to BM-MSC that relies on the shedding of AREG at the surface of cancer cells, thereby promoting cancer invasion.

Material and Methods

Animal Studies

All animal experiments were conducted in accordance with the guidelines of the local ethical committee of the University of Liège (Belgium).

Metastasis Experiment. Six- to eight-week-old female C57BL/6 mice (Janvier Laboratories, Saint-Berthevin, France) were subcutaneously injected (in the two flanks) with LLC cells (1×10^5) alone or with BM-MSCs (5×10^5). Tumor growth was evaluated by measuring luciferase bioluminescence at days 7, 9, 12, and 14 after injection using the bioluminescent IVIS imaging system (Xenogen-Caliper, Hopkinton, MA). At day 14 after cell injection, the primary tumor masses were excised, and metastases were monitored *in vivo* weekly by using the bioluminescent imaging system. At 35 days after injection, the mice were sacrificed, and the organs (lung, liver, ovary, kidney, intestine, and pancreas) were checked *ex vivo* for metastatic colonization through bioluminescence detection.

Tumor Kinetic Experiment. The mice injected as described above were sacrificed at 7, 9, 12, and 14 days postinjection. For the visualization of functional vessels, 200 μl of FITC-dextran (2.5 mg/ml in PBS) (Sigma Aldrich, St Louis, MO) was intravenously injected 3 minutes before sacrifice. Tumors were weighed, and histopathological analyses were performed as described below.

Measurement of Hemoglobin Content

Tumors resected at day 14 postinjection were lyophilized, and the hemoglobin content was determined by using Drabkin's reagent according to the manufacturer's instructions (Sigma Aldrich). The amount of hemoglobin was normalized to the weight of the lyophilized tumor. The data presented are those of two independent experiments.

Cell Lines, Recombinant Proteins, and Blocking Antibodies

The luciferase-expressing LLC (Luc-LLC) cell line of the C57BL/6 background was purchased from Caliper Lifesciences (Xenogen-Caliper). Luc-LLC cells were cultured in Dulbecco's modified Eagle's medium (DMEM; Gibco Invitrogen Corporation, Paisley, United Kingdom) supplemented with 10% heat-inactivated fetal bovine serum (FBS), 2 mM glutamine, 100 UI/ml penicillin/streptomycin, and 1 mg/ml geneticin [selective antibiotic (Serva GmbH, Heidelberg, Germany)] and maintained in a humidified incubator at 37°C in a 5% CO_2 atmosphere. We used commercially available, recombinant AREG (R&D Systems, Minneapolis, MN); TAPI-0 (Calbiochem, San Diego, CA), which is an inhibitor of TACE; and AG1478 (Calbiochem), an inhibitor of EGFR.

Mesenchymal Stem Cell Isolation and Characterization

MSCs were isolated from the BM of either C57BL/6J or transgenic mice that were heterozygous for the enhanced green fluorescent protein (eGFP) under the control of the β-actin promoter C57BL/6-Tg(ACTbEGFP)10sb (Jackson Laboratories, Bar Harbor, ME). Mouse tibiae and femurs were carefully cleaned and crushed in a mortar, and the BM was recovered with phosphate-buffered saline (PBS) containing 2% FBS and 1 mM EDTA. Mononuclear cells were isolated using Ficoll (GE Healthcare Bioscience AB, Uppsala, Sweden). Cells were rinsed twice with PBS and then seeded in complete Mesencult medium (Stem Cell Technologies, Grenoble, France). After 3 days of culture at 37°C, nonadherent cells were removed, and the adherent layer was cultured until it reached 70% to 80% confluence. The mesenchymal cell population was further purified by negative selection with the "mouse hematopoietic progenitor stem cell enrichment set" (BD Bioscience, Berdford, MA, USA). The MSC phenotype was characterized by immunostaining and flow cytometry (FACS) analysis. Osteogenic and adipogenic differentiation assays were also performed on the MSCs, as previously described [23].

Culture Conditions and Preparation of Conditioned Medium

LLC cells were cultured alone (monoculture), with a direct cell mixture of BM-MSCs (direct co-culture), or in a Transwell chamber (pore 0.4 μm; Greiner BioOne, Frickenhausen, Germany) in which the two cell types were separated by a semipermeable membrane (1:5 ratio) (indirect co-culture). Two days after cell seeding, the cells were starved for 1 hour with serum-free DMEM, and the medium was replaced with fresh, serum-free DMEM. After 24 hours, the conditioned medium (CM) was collected, centrifuged at 1000*g* for 10 minutes, and concentrated 10× with Amicon Ultra Centrifugal Filters 10K (Millipore, Cork, Ireland). CM aliquots were stored at −20°C until use.

Proliferation Assay

For the proliferation assays, BM-MSC (6×10^4 cells/well) and Luc-LLC cell (3×10^4 cells/well) monocultures, direct co-cultures, or indirect co-cultures were seeded in 24-well plates in DMEM containing 2% FBS. After 3 days, 150 μg/ml of luciferine (Promega, Madison, WY) was added to each well, and plate images were collected for 10 seconds to 1 minute using the IVIS imaging system (Xenogen-Caliper). Photons emitted from tumor cells were quantified using the Living Image software (Xenogen-Caliper). The suitability of this assay was assessed by seeding an increased number of LLC cells in the presence or absence of BM-MSCs, leading to an output signal that was directly correlated with the number of seeded cells.

Spheroid Assay

Multicellular spheroids were generated by seeding LLC cells (1×10^3) alone or with BM-MSCs (5×10^2) in each well of a nonadherent, round-bottomed plate (Greiner BioOne) in DMEM containing 2% FBS and 0.24% high-viscosity methyl cellulose (Sigma Aldrich). After 24 hours of culture, spheroids (maximum 8/well) were collected, embedded in type I collagen gels (1.25 mg/ml; BD Biosciences) in 24-well plates, and maintained in 2% FBS-DMEM at 37°C for 24 hours. In some assays, collagen gels (1.25 mg/ml, BD Biosciences) were preincubated before spheroid embedding with the following compounds: a neutralizing anti-AREG antibody (3 µg/ml, R&D Systems), a normal goat IgG control (3µg/ml, R&D Systems), an EGFR inhibitor, AG1478 (20 µM, Calbiochem), and a TACE inhibitor, TAPI-0 (10 µM, Calbiochem) Cells were examined under a Zeiss Axiovert 25 microscope equipped with an Axiocam Zeiss camera and KS 400 Kontron image-analysis software (Carl Zeiss Microscopy, Zaventem, Belgium).

Image Analysis and Computerized Quantification

Image processing and measurements were implemented using the image analysis toolbox of Matlab 7.9 (Mathworks, Natick, MA) according to the following steps. Morphological filters [24] were first applied to correct uneven illumination in the collagen background and to eliminate noise. Cells were then segmented using an automatic threshold [25]. The convex envelope, defined as the minimal convex polygon that contained the whole spheroid, was automatically determined. Finally, the convex envelope area, defined as the number of pixels belonging to the convex envelope multiplied by the pixel size (in mm^2), was measured for each spheroid.

RNA Extraction and Reverse Transcription–Polymerase Chain Reaction (RT-PCR)

Total RNAs from BM-MSCs and LLC cells were extracted using the High Purity RNA isolation kit (Roche, Mannheim, Germany) according to the manufacturer's protocol. RT-PCR was performed on 10 ng of total RNA using an amplification kit (GeneAmp Thermostable rTth Reverse Transcriptase RNA PCR Kit; Roche). The RT-PCR products were resolved in 10% acrylamide gels and analyzed with a fluorescence imager (LAS-4000; Fujifilm, Tokyo, Japan) after staining with Gel Star (Cambrex, East Rutherford, NJ). The gene expression levels were measured as the ratio between expression values and internal 28S. Statistical significance of differences between the observed values was evaluated using the Mann-Whitney test.

Western Blotting

Cells or tumors were lysed for 30 minutes in ice-cold lysis buffer (1% Triton X-100, 150 mM NaCl, 1% IGEPAL-CA 630, 1% Na deoxycholate, 0.1% sodium dodecyl sulfate, complete). To achieve homogenization, tumor extracts were placed in tubes containing ceramic beads (Magna Lyser Green Beads; Roche) in a Magna Lyser (Roche). Cell lysates were clarified by centrifugation at 12000 rpm at 4°C for 30 minutes and stored frozen at –20°C. The protein concentrations were determined using the DC Protein Assay kit (Bio-Rad Laboratories, Hercules, CA), and protein samples were resolved on sodium dodecyl sulfate polyacrylamide gels and subsequently transferred to polyvinylidene fluoride membranes. The membranes were treated with blocking buffer (PBS with 0.1% Tween-20; Merck, Darmstadt, Germany, and 1% casein; Sigma Aldrich) for 1 hour at room temperature before overnight incubation

at 4°C with primary antibodies raised against mouse AREG (1/500, goat anti-mouse IgG; R&D Systems) or mouse TACE (1/500, rabbit anti-mouse IgG; Millipore). After washings, the membranes were incubated for 1 hour with secondary horseradish peroxidase antibodies (1/3000, donkey anti-goat/HRP; Santa-Cruz Biotechnology, Inc., Santa Cruz, CA, or 1/2000, goat anti rabbit/HRP; DakoCytomation, Glostrup, Denmark), and proteins were detected by chemiluminescence using an enhanced chemiluminescence kit (Perkin Elmer Life Sciences, Boston, MA) according to the manufacturer's instructions. Subsequent detection of actin (rabbit anti-actin; Sigma Aldrich) was performed on the same filters as the loading control.

Cytokine Array and AREG ELISA

A "Proteome Profiler, Mouse Angiogenesis Array kit" was applied on medium conditioned by cells according to the procedure recommended by the manufacturer (R&D Systems). The quantification was performed by detecting chemiluminescence (LAS-4000, Fujifilm). For a specific dosage of AREG, a DuoSet ELISA Development kit (R&D Systems) was used following the manufacturer's instructions.

TACE Activity Assay Using a Fluorescence Resonance Energy Transfer (FRET) Peptide

The TACE activity level was assessed using a peptide-based FRET assay and a peptide purchased from Peptides International (Louisville, KY) as substrate: Abz-Leu-Ala-Gln-Ala-Val-Arg-Ser-Ser-Ser-Arg-Dap(Dnp)-NH$_2$. Upon cleavage by TACE, the fluorescence of Abz (2-aminobenzoyl), which was quenched by Dnp (2,4-Dinitrophenyl), was recovered and monitored at λ_{ex} = 320 nm and λ_{em} = 420 nm. For this assay, LLC cells and/or BM-MSCs (1:5 ratio) were incubated in a 96-well plate in DMEM containing 2% FBS. After 24 hours, the FRET peptide was added (10 µM) to each well. DMEM containing 2% FBS without cells was used as a control. The fluorescence was monitored every 30 minutes during 2 hours (SpectraMaxi3; Molecular Devices, Obergausen, Deutschland).

Immunohistochemistry

The immunohistochemical analyses were performed on paraffin sections using anti-GFP antibody (Abcam, Cambridge, United Kingdom) to stain GFP-expressing BM-MSCs and anti-FITC antibody (Roche) to detect functional vessels (dextran/FITC). Virtual images were acquired using the fully automated, digital microscopy system dotSlide (BX51TF; Olympus, Aartselaar, Belgium) coupled with a Peltier-cooled, high-resolution digital color camera (1376 × 1032 pixels; XC10; Olympus). The images of the whole tissue sections were digitized at high magnification (×100), producing virtual images with pixel sizes of 1.510 µm. On these digital images, vessels were drawn manually and transformed to obtain a binary image in which pixels representing vessels had intensity equal to 1 and those corresponding to the background intensity had intensity equal to 0. The number of vessels on those binary images was measured automatically. The results are expressed as the unity of the area of tumor tissue. Image analysis was conducted using the Matlab 7.9 software (Mathworks).

TACE Knockdown

BM-MSCs were transfected with LNA-GapmeRs (Exiqon, Vedbaek, Denmark) targeting one common sequence of three variants of TACE: 5 -GAGTTACAGAGTTGA-3 , referred as "Gap TACE". As negative control, a nonhomologous sequence

("Gap CTRL") was designed: 5 -AACACGTCTATACGC-3 . Cells were transfected by using interferin according to the manufacturer's instructions (Polyplus, Leuven, Belgium). TACE mRNA expression and enzymatic activity were analyzed 72 hours after transfection.

Statistical Analysis

Data were analyzed with GraphPad Prism 5.0 (San Diego, CA). The appropriate test was used [linear regression, chi squared, Student's *t* test or Mann-Whitney (for non-Gaussian distribution)] to determine the significance ($P < .05$) of differences between experimental groups (*$P < .05$, **$P < .01$, ***$P < .001$).

Results

BM-Derived MSCs Enhance tumor Growth and Metastasis Formation In Vivo

MSCs were isolated from the BM of C57BL/6J mice or mice expressing eGFP (C57BL/6-Tg(ACTbEGFP)10sb). Mononuclear cells were collected using a Ficoll-Paque density gradient centrifugation. Nonadherent cells were removed after 3 days of culture in a specific stem cell medium. After depletion through magnetic cell separation of CD45- and CD11b-positive cells, BM-derived cells were characterized using flow cytometry (FACS) and differentiation assays. Those cells expressed the surface marker profile typical for MSC: SCA-1 and CD106. Furthermore, we confirmed the negativity for CD45 and CD11b, and a low positivity for CD34 [23]. After culture under adipogenic and osteogenic differentiation conditions, cells were stained using red oil or alizarin red to confirm their differentiation potential. The accumulation of intracellular lipid droplets and the deposition of extracellular calcium phosphate were observed. Based on their phenotype and the multilineage differentiation potential, cells isolated from murine BM display the typical features of MSC [23]. The functional impact of the heterotypic interactions that occurred between LLC cells and BM-MSCs was evaluated *in vivo* by co-injecting GFP-positive BM-MSCs and luc-LLC cells into syngeneic C57BL/6J mice. Primary tumor growth was followed *in vivo* by LLC cell luminescence signal quantification using the *in vivo* imaging system IVIS 200 (Figure 1A). Mice co-injected with LLC cells and BM-MSCs exhibited accelerated tumor growth compared with mice injected with LLC cells alone (Figure 1B). This led to a two-fold increase in tumor volume at day 14 (Figure 1C). At this time point, the primary tumors were removed, and the emergence of metastases was quantified. At day 35, the incidence of lung metastases was also higher in mice co-injected with LLC cells and BM-MSCs (Figure 1, D–F). The injections with BM-MSCs alone did not result in tumor formation (data not shown).

A kinetic study was conducted to investigate the fate of BM-MSCs within LLC tumors after 7, 9, 12, or 14 days. The number of injected BM-MSCs observed in the tumor stroma decreased drastically over time, and only few GFP+ BM-MSCs were still detected at day 14 and are part of the initial injected cells (Figure 2A). Interestingly, in our model, the presence of BM-MSCs did not affect functional blood vessel formation, as assessed by FITC-dextran detection of blood endothelial cells and hemoglobin content measurement (Figure 2, B and C).

BM-MSCs Increase LLC Cell Proliferation and Invasion In Vitro

Taking advantage of the luciferase expression by LLC cells, the proliferation of LLC cells was evaluated by bioluminescence detection after luciferin administration. Three conditions were tested: 1) LLC

cells alone, 2) LLC directly co-cultured with BM-MSCs, and 3) co-culture of LLC cells separated from BM-MSCs by a semipermeable membrane to avoid direct cell–cell contacts (Figure 3A). In direct 2D co-cultures, the LLC cell number was significantly increased after 72 hours of culture, whereas tumor cell proliferation was not affected in indirect co-culture conditions (Figure 3B). In a 3D spheroid invasion assay, LLC cell invasive properties were stimulated when tumor cells were mixed with BM-MSCs compared with the invasion of LLC cells as monospheroids (Figure 3C). The use of GFP-expressing BM-MSCs in this assay demonstrated that the migrating cells were LLC cells rather than BM-MSCs (Figure 3C). Indeed, GFP-positive cells remained inside the spheroid, whereas LLC cells were able to spread out and invade the surrounding type I collagen matrix.

AREG Shedding Requires a Contact Between LLC Cells and BM-MSCs

To examine the molecular mechanism underlying BM-MSC–mediated promotion of tumor invasiveness, we carried out monocultures of each cell type, and direct or indirect co-cultures of LLC cells and BM-MSCs (Figure 4A). The media conditioned by these different cultures were screened for a panel of cytokines, chemokines, and growth factors using a protein array. In most cases, the resulting levels of secreted proteins reflected the additive production of each cell type cultured alone. Interestingly, we noticed that AREG amount was three times higher in direct co-cultures than in monocultures. Moreover, close physical contacts between LLC cells and BM-MSCs were required to stimulate AREG secretion because no variation in AREG amount was observed in indirect co-cultures (Figure 4B).

AREG regulation was next analyzed at the mRNA and protein levels using RT-PCR and Western blot analyses, respectively. AREG mRNAs were mainly expressed by LLC cells, and their levels were significantly increased upon direct co-culture with BM-MSCs (Figure 4C). Whereas the AREG protein level was not modulated in the cell extracts of direct co-cultures (Figure 4C), the secreted form of AREG was increased in the medium conditioned by direct co-cultures, but not by indirect co-culture, confirming the importance of close cell–cell contacts (Figure 4D). Consistently, ELISA analyses revealed a three-fold increase in the secretion of AREG in conditioned media of direct co-cultures compared with that observed in monocultures or indirect co-cultures (Figure 4E). These data suggest that BM-MSCs enhanced AREG secretion, likely through a posttranslational mechanism, which could rely on shedding of the proform into its soluble form. The modulation of AREG production that was observed *in vitro* was confirmed *in vivo* by Western blotting performed on tumor extracts (Figure 4F). Interestingly, the AREG contents were increased in tumors induced by the LLC+BM-MSC mixture compared with those induced by the LLC cell injection alone.

AREG Shed from LLC Cells Contributes to LLC Cell Invasion

The functional consequence of AREG production on cancer cell invasion was next evaluated *in vitro* in multicellular LLC spheroids invasion assay treated with increasing concentrations of recombinant AREG (recAREG). A high concentration of recAREG (200 ng/µl) stimulated the invasion of LLC cells (Figure 5A). Similarly, the medium conditioned by LLC cells directly co-cultured with BM-MSCs, containing high amount or AREG as assessed by ELISA, enhanced LLC cell sprouting from the spheroid. Notably,
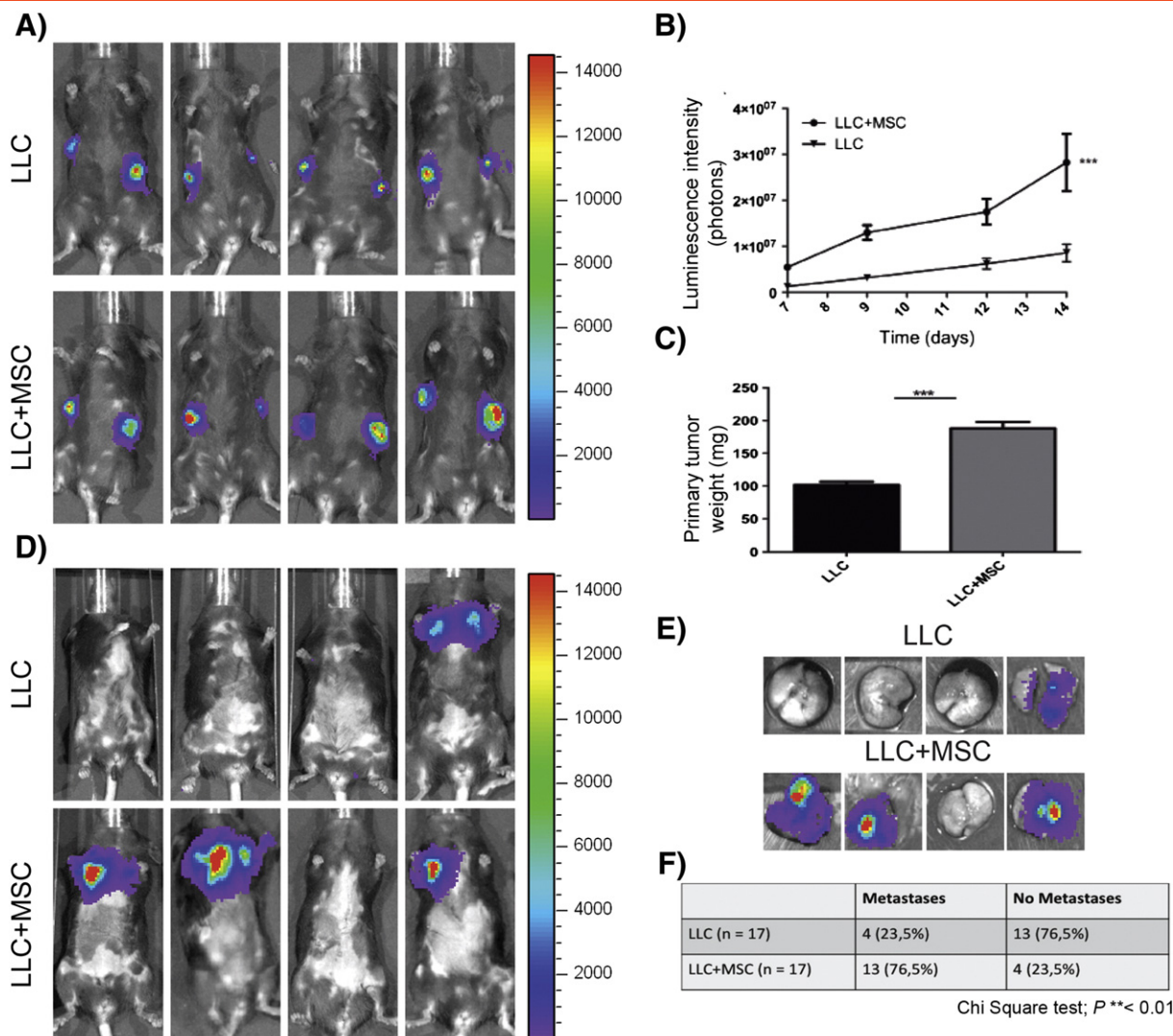
Figure 1. MSCs enhance tumor growth and metastasis formation.Luc-LLC cells (1×10^5) were subcutaneously injected into C57BL/6J mice in both flanks in the absence (LLC) or presence of BM-MSCs (5×10^5) (LLC+MSC). Representative data from three independent experiments are shown. (A) *In vivo* bioluminescent signal of the primary tumors at day 14 post cell injection ($n = 17$ per group). (B) Quantification of the luminescent signal as a function of time after cell injection ($n = 17$ per group; linear regression ***$P < .001$). (C) Weights of primary tumors resected at day 14 ($n = 17$ per group; Student's *t* test ***$P < .001$). (D) *In vivo* bioluminescent signal of lung metastases at day 35. (E) Representative *ex vivo* bioluminescent signal of lungs resected from mice at day 35. (F) Statistical analysis of metastasis incidence at day 35 (chi-square test **$P < .01$).

this proinvasive effect was abrogated by an AREG-specific blocking antibody and not by a control antibody (Figure 5*B*). Moreover, the proinvasive effect of BM-MSCs on LLC cells was abrogated by the incubation of heterospheroids (LLC+MSC) with AG1478 (20 μM), a specific inhibitor of EGFR (Figure 5*C*).

TACE Produced by BM-MSCs Is Necessary to Increase AREG Secretion by LLC

TACE is the main protease implicated in AREG shedding [26]. We thus investigated how this protease was involved in the shedding of AREG induced by BM-MSCs. LLC cells and BM-MSCs both expressed TACE mRNAs, but no transcriptional modulation was observed when BM-MSCs were co-cultured with LLC cells (Figure 6*A*). Using Western blotting, we detected two forms of TACE: a pro-TACE species of 130 kDa and activated TACE forms of 80 kDa, corresponding to glycosylated and nonglycosylated forms.

Although no modulation of these two forms was observed *in vitro*, increased amounts of active TACE were detected *in vivo* in xenografts generated by LLC+BM-MSC mixture injection compared with LLC tumors (Figure 6, *B* and *C*). The activity of TACE was next analyzed *in vitro* by FRET to determine whether the detection of active TACE by Western blot correlates to proteolytic activity at the cell surface. Cells were incubated with a FRET peptide, which is a specific substrate for TACE. Upon hydrolysis by TACE, a fluorescent signal proportional to TACE activity is emitted. Little TACE activity was observed in LLC cells. However, higher TACE activity was detected in monoculture of BM-MSCs, and upon direct co-culture of LLC+BM-MSCs, this activity was increased. In addition, the activity of TACE was decreased using TAPI-0, an inhibitor of TACE, and after BM-MSC transfection with anti-TACE GapmeR (Figure 6*D*). As expected, the release of AREG in CM was also decreased after TAPI-0 treatment or in co-culture with MSC Gap TACE
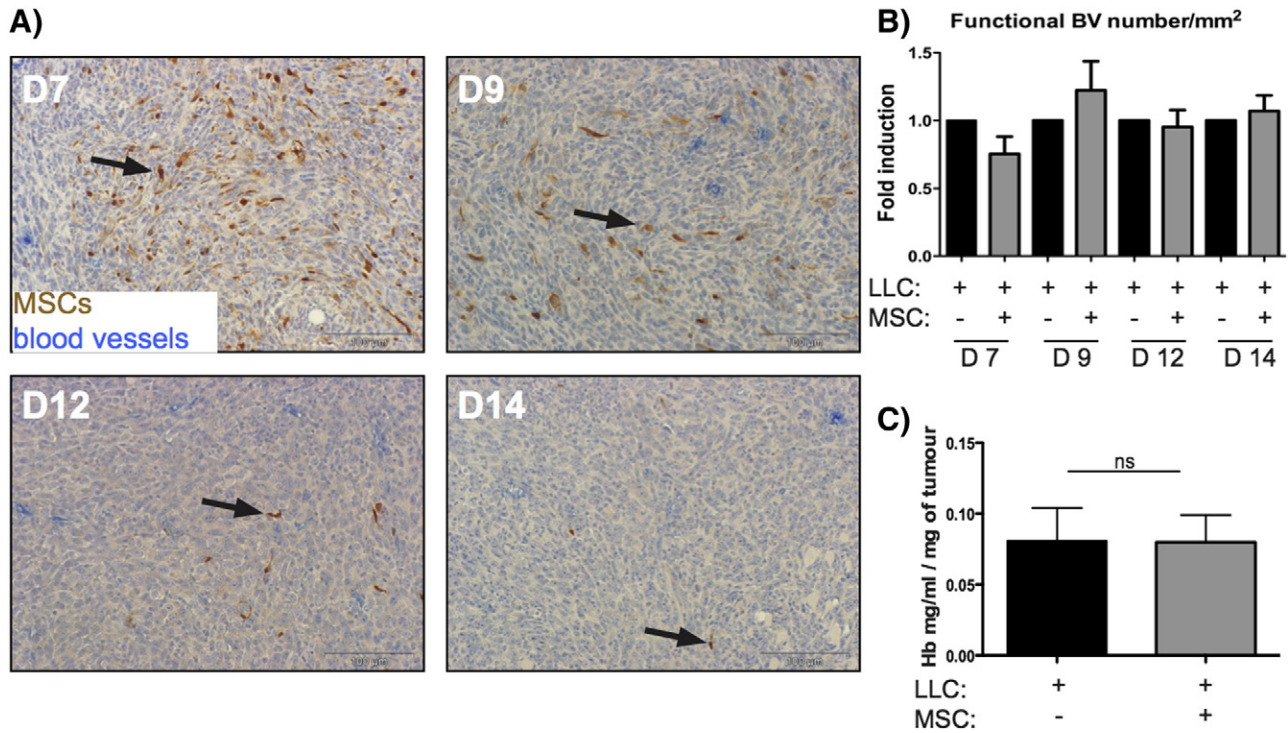
Figure 2. GFP-labeled BM-MSCs co-transplanted with tumor cells do not affect the vascular density within a tumor mass.Luc-labeled LLC cells (1×10^5) were subcutaneously injected in C57BL/6J mice in the absence (LLC+; MSC−) or presence of GFP-expressing BM-MSCs (5×10^5) (LLC+; MSC+). Primary tumors were resected at 7, 9, 12, and 14 days (D7-D14) immediately after mice injection with dextran-FITC. (A) Immunodetection of GFP in BM-MSCs (brown) and FITC (vessels in blue) on paraffin sections of tumor tissues. (B) Quantitative analysis of the vessel density in tumors. Data are expressed as the fold induction of the functional blood vessel (BV) number per mm^2 that was observed within the primary tumor mass. (C) Measurement of the hemoglobin content in tumors. The amount of hemoglobin was normalized to the weight of the lyophilized tumor ($n = 10$ per group, ns = no statistical difference).
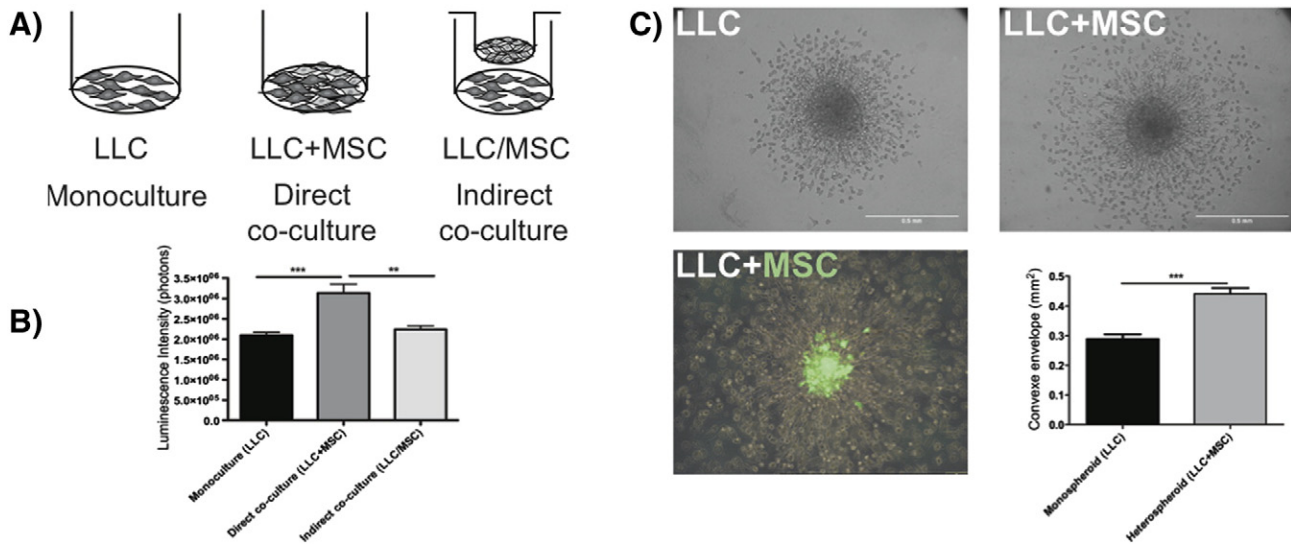

Figure 3. BM-MSCs promote LLC cell proliferation and invasion.LLC cells were cultured alone (LLC, monoculture) or co-cultured with MSCs (LLC+MSC) in direct contact (direct co-culture) or separated by a semipermeable membrane in a transwell chamber (LLC/MSC, indirect co-culture). Cells were either seeded on plastic (A, B) or embedded as spheroids in a collagen gel (C). (B) Quantitative analysis of the luminescence intensity of Luc-LLC cells cultured for 3 days with or without BM-MSCs (Mann-Whitney: **$P < .01$; ***$P < .001$). (C) The invasion of LLC cells in the 3D spheroid model is increased in the presence of BM-MSCs (LLC+MSC) (Mann-Whitney: ***$P < .001$). In the lower panel, the spheroid is composed of LLC cells and GFP+ BM-MSCs, revealing that only cancer cells migrate into the matrix, whereas BM-MSCs remain in the spheroid (green cells). The graph corresponds to the quantification of cell invasion.
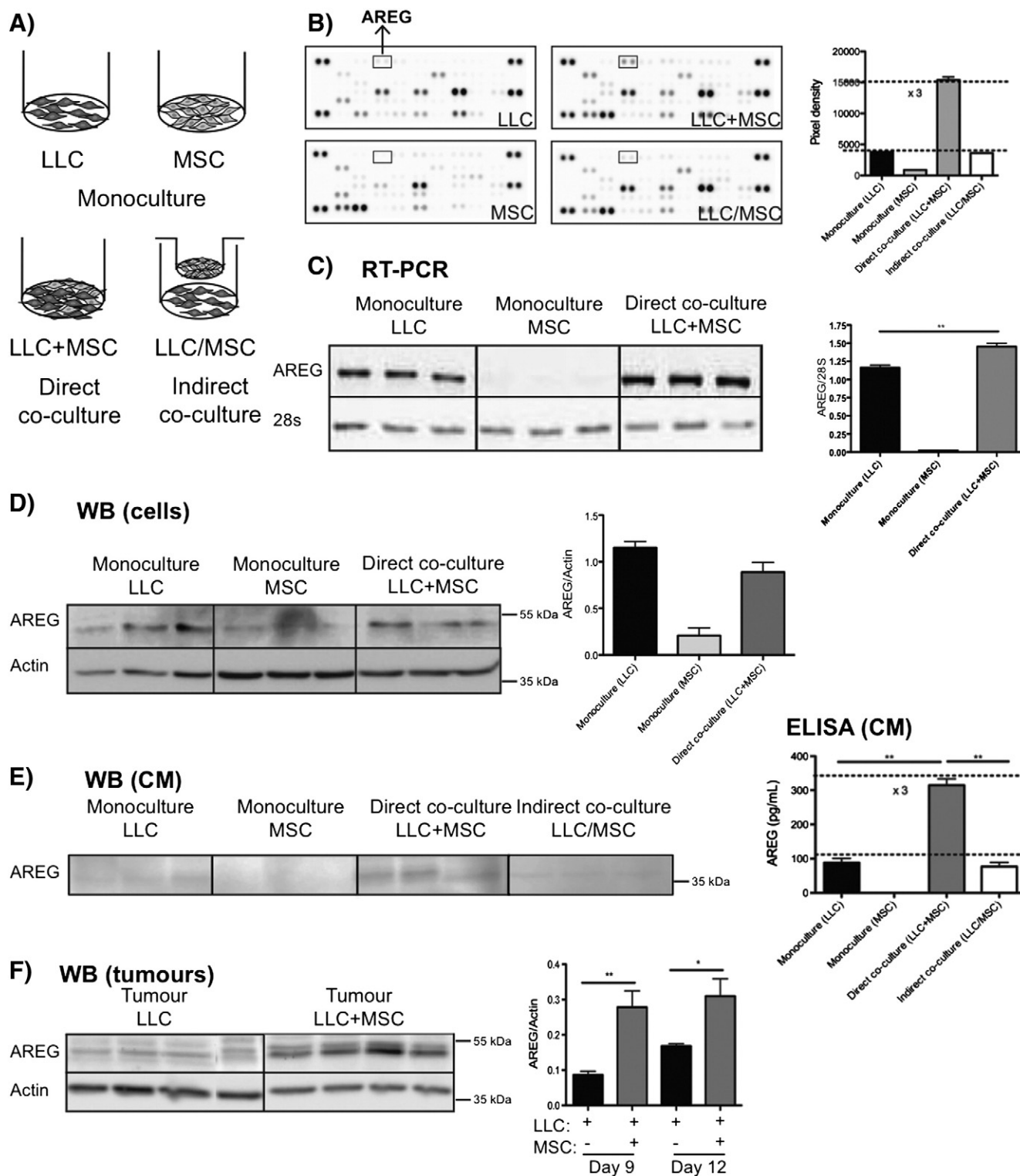
Figure 4. BM-MSCs enhance AREG secretion from LLC cells.LLC cells and BM-MSCs were cultured for 3 days, either alone (monoculture), together (direct co-culture), or separated by a semipermeable membrane to avoid cell–cell contacts (indirect co-culture), as schematically presented (A). The results presented are those of one representative assay out of at least three experiments using different primary BM-MSC cultures. (B) The level of AREG in conditioned media is compared using a cytokine array. (C) RT-PCR analysis of AREG mRNA expression. The results are expressed in arbitrary units corresponding to the AREG/28S ratio (Mann-Whitney: **$P < .01$). (D) Western blot analysis of the AREG production in culture lysates. Production of the actin protein is included as a loading control. The graph corresponds to the quantification of AREG production by scanning densitometry. The results are expressed as the AREG/actin ratio. (E) Secreted levels of AREG analyzed by ELISA (right panel) and by Western blotting (left panel) on conditioned medium from LLC cells, BM-MSCs, and direct or indirect co-cultures of LLC cells and BM-MSCs. (F) Western blot analysis of tumors resected 9 or 12 days after injection of LLC cells with or without BM-MSCs (Mann-Whitney: *$P < .05$, **$P < .01$). Actin is used as a loading control, and data are presented as the AREG/actin ratio.
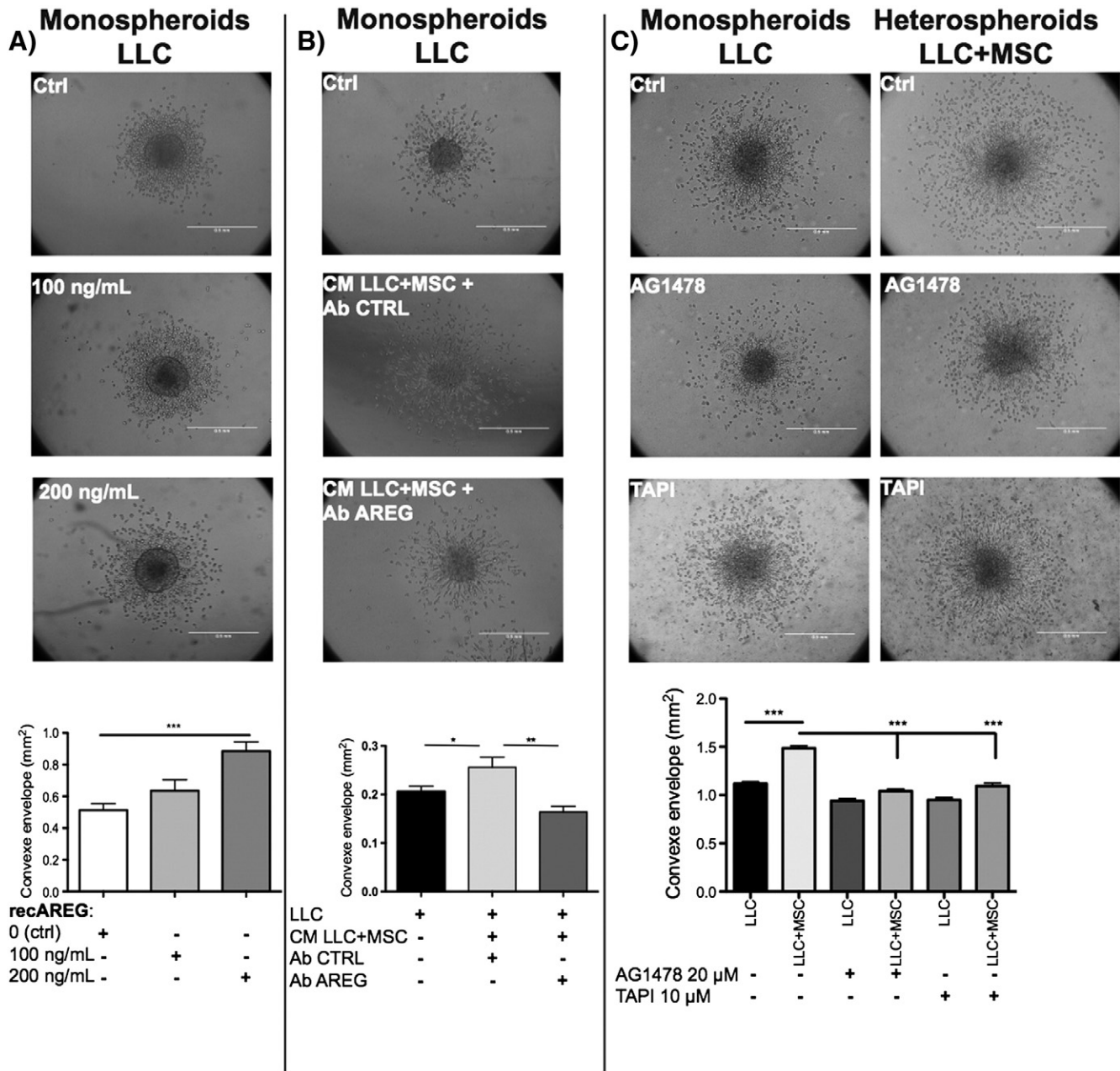
Figure 5. AREG present in co-cultures of MSC+LLC-conditioned media enhances tumor cell invasion in a 3D spheroid model.LLC cells were cultured as monospheroids (LLC) without or with medium conditioned by co-cultured cells (CM LLC+MSC) or co-cultured with BM-MSC in heterospheroids (LLC+MSC). (A) Increasing concentrations of recombinant AREG (recAREG) were added to monospheroid cultures. (B) A control antibody (Ab Ctrl) or an anti-mouse AREG-blocking antibody (Ab AREG) was preincubated overnight at 4°C with the conditioned medium. The stimulation of LLC cell invasion by co-culture–conditioned medium (CM LLC+MSC) is abrogated upon a preincubation with an AREG-blocking antibody. (C) Monospheroids (LLC) and heterospheroids (LLC+MSC) were incubated with an inhibitor of EGFR (AG1478, 20 μM) or an inhibitor of TACE (TAPI-0, 10 μM). The graph corresponds to the quantification of cell invasion (Student's t test: *$P < .05$, **$P < .01$; ***$P < .001$).

(Figure 6*E*). Interestingly, TAPI-0 also blocked the proinvasive effect of BM-MSC on LLC cells in a collagen gel (Figure 5*C*).

Discussion

Although the effects of MSCs on tumor cell invasion have been recently described, the complex cross talk established between both cell types is still unclear and poorly documented. We herein provide evidence that the direct confrontation of BM-MSCs with LLC cells significantly increases *in vivo* tumor growth and lung colonization as well as *in vitro* tumor cell proliferation and invasion. In this study, we identify a new juxtacrine signaling pathway involving the contact between membrane-associated proteins present at the surface of stromal cells (TACE) and adjacent tumor cells (pro-AREG). The tumor-derived soluble AREG shed by the stromal TACE then acts in an autocrine and/or paracrine manner on cancer cells and stimulates invasiveness.

Growing evidence supports the importance of paracrine interactions occurring between cancer cells and MSCs, which involve growth
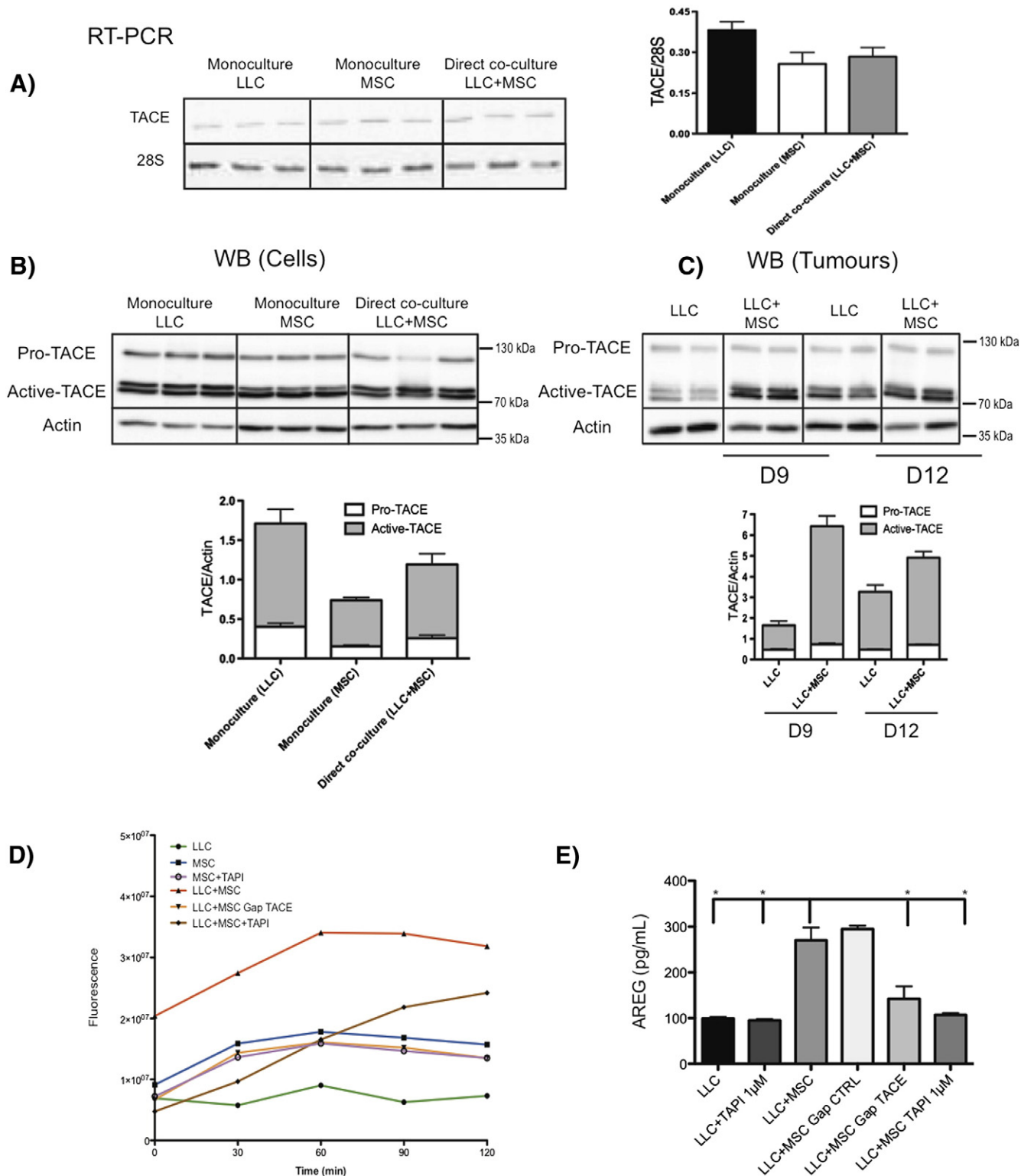
Figure 6. Active TACE is increased in the presence of BM-MSCs and is responsible for AREG shedding.(A) RT-PCR analysis of TACE expression. The results are expressed in arbitrary units corresponding to the ratio between ADAM17/28S. (B, C) Western blot analysis of pro- and active-TACE production *in vitro* in culture lysates (B) and *in vivo* in tumors induced by LLC cells with or without BM-MSCs (C). Actin is included as a loading control. The graph corresponds to the quantification of TACE production by scanning densitometry. The ratio of pro-TACE/actin and active TACE/actin reveals a significant increase in active-TACE production when BM-MSCs are present in tumors at days 9 ($P = .0002$) and 12 ($P = .104$) after injection. LLC cells and/or BM-MSCs were cultured alone or in co-cultures treated with TAPI-0 (1 μM) or control. BM-MSCs transfected with anti-TACE or control GapmeR were also used. (D) TACE activity was evaluated by FRET at different time points (0 to 2 hours) (linear regression: ***$P < .001$). (E) AREG amounts were determined in the conditioned medium using ELISA (Mann-Whitney: *$P < .05$).

factors, angiogenic factors, and/or cytokines, among which SDF-1 and CCL5 emerged as key players [6,27,28]. The originality of our work relies on the demonstration that juxtacrine stromal tumor cell interactions lead to the release of soluble AREG from the tumor cell membrane through TACE activity located at the MSC membrane. AREG secretion was increased only when cancer cells were in direct contact with BM-MSCs but not when they were separated by a semipermeable membrane avoiding cell–cell contacts. The increased AREG amounts that were detected in co-cultures are ascribed to AREG shedding from the tumor cell surface rather than to a transcriptional regulation of its gene expression, as assessed by RT-PCR, Western blotting, and ELISA analyses. In *in vitro* assays, LLC cell invasion was increased by the addition of medium conditioned by BM-MSC+LLC co-cultures. Furthermore, this proinvasive effect was abrogated by blocking antibodies targeting AREG, demonstrating the contribution of AREG to cancer cell invasion.

AREG is overexpressed in cancerous tissues such as human colon, stomach, breast, and pancreas [20]. The role of AREG in cancer development and progression is supported by clinical data showing that AREG levels are correlated with tumor progression and poor patient survival and may serve as a prognostic biomarker, for instance, for non–small cell lung carcinoma [29–32]. Depending on the cellular context, AREG can exert diverse effects that affect tumor progression such as self-sufficiency in growth signals, tissue invasion, and evasion of apoptosis [20]. Its role in tumor initiation and/or progression is inextricably linked to that of its receptor, EGFR. The binding of AREG to EGFR induces autophosphorylation of the EGFR intracellular tyrosine kinase domain leading to MEK/ERK1/2, PI3K/AKT, and STAT3 pathway activation. Consequently, cancer cells are endowed with proliferative, migrative, and invasive properties through EGFR activation [20,33]. The soluble AREG form that is shed from LLC cells acts in an autocrine or paracrine manner on cancer cells expressing EGFR to enhance their motility and invasive potential. This conclusion is supported by the use of an EGFR inhibitor in the invasive assay. It is worth noting that soluble AREG has been described as a more potent factor than membrane-anchored AREG in mammary epithelial cells [34]. Our data are in line with previous studies reporting that AREG increased the motility of different cell lines, including MCF-7, SUM-149, and MDA-MD-231 breast cancer cells [35,36]. AREG also appears to contribute to actin rearrangement through E-cadherin redistribution [37,38]. Furthermore, AREG can induce the expression of factors involved in matrix degradation, such as matrix metalloproteinases (MMP-2, MMP-9) [36,39,40]. In our spheroid invasion assay, the MMP inhibitor Ro28-2653, which does not block TACE [41], reduced the cell invasion from monospheroids composed of LLC cells alone or heterospheroids composed of BM-MSCs and LLC cells to a similar extent (data not shown). These data suggest that, in our model, the BM-MSC-mediated effect on cancer cell invasion was independent on MMP status. The blockade of AREG shedding by TAPI, an inhibitor of TACE, supports the implication of TACE in our model. Importantly, increased AREG secretion was associated with enhanced active-TACE detection in primary tumors composed of LLC+BM-MSC mixture as compared with primary tumors composed of LLC cells alone. Arguing for the importance of MSC-derived TACE, TACE activity was detected *in vitro* through a specific FRET analysis in BM-MSCs but not in LLC cells. The poor TACE activity detected in LLC cells while the enzyme was detected by Western blot is intriguing. However, several studies have reported

that protein levels of TACE do not directly correlate with the protein activity [42–44]. Rather than depending on the simple removal of its inhibitory prodomain, TACE activity seems to be readily switched « on and off » at the cell surface [45]. The mechanism by which TACE becomes catalytically active remains poorly understood [26,46]. In the current work, increased TACE activity was detected in LLC+MSC direct co-cultures as compared with monocultures. Importantly, this activity was inhibited by TAPI. The transfection of BM-MSCs with anti-TACE GapmeRs confirms that the increased TACE activity relies on the BM-MSC–derived enzyme. Our data also suggest that TACE activity on BM-MSCs requires an activation in the presence of cancer cells through physical contact between both cell types [46].

Our work is uncovering novel features of the complex dialogue established between BM-MSC and tumor cells. It establishes an unprecedented link between BM-MSC and AREG. We here assign a novel function to BM-MSC consisting of the shedding of AREG at the surface of tumor cells leading to proinvasive and metastatic features. The originality of our finding relies on the observation that AREG shedding occurs in *trans*, with MSC-derived TACE acting on AREG expressed by tumor cells. A *trans*-shedding has been previously reported for ADAM10 in ephrin cleavage involving only one cell type [47]. To the best of our knowledge, this is the first report of TACE acting in *trans* in a tumor cell–host cell dialogue. Although AREG shedding has already been reported in tumor cells–(myo)fibroblast interactions, the shed AREG was shown to act in a paracrine manner on cancer cells [48,49]. In the present study, we define an unprecedented link between MSC and AREG implicating a *trans*-shedding of pro-AREG at the tumor cell surface. It is worth noting that BM-MSCs within the tumor stroma can differentiate into CAFs [12,50,51], which secrete several cytokines. In line with our data, a recent study has reported increased expression of TACE in CAFs extracted from human breast carcinomas compared with donor-matched normal fibroblasts [52]. In a recent elegant study using colorectal cancer cells [53], BM-MSCs were reported to secrete neuregulin, another ligand of EGFR, and this was associated with poor prognosis [53]. In contrast to our study, neuregulin was expressed by BM-MSCs rather than by tumor cells, and cell–cell contacts were not required to stimulate colorectal cancer progression. Altogether, these studies shed light on the multifaceted dialogue that occurs between BM-MSCs and tumor cells that contribute to the tumor promotion.

In conclusion, we provide the first evidence of juxtacrine interactions between BM-MSCs and cancer cells that increase the release of soluble AREG from cancer cells and contribute to the invasive properties of tumor cells. Strategies developed to interfere with the AREG activation loop initiated by MSC and tumor cell interactions might be of therapeutic value to prevent cancer progression and invasion.

References

[1] Joyce JA and Pollard JW (2009). Microenvironmental regulation of metastasis. *Nat Rev Cancer* **9**, 239–252.

[2] Hanahan D and Weinberg RA (2011). Hallmarks of cancer: the next generation. *Cell* **144**, 646–674.

[3] Quail DF and Joyce JA (2013). Microenvironmental regulation of tumor progression and metastasis. *Nat Med* **19**, 1423–1437.

[4] Quante M, Tu SP, Tomita H, Gonda T, Wang SS, Takashi S, Baik GH, Shibata W, Diprete B, and Betz KS, et al (2011). Bone marrow–derived myofibroblasts contribute to the mesenchymal stem cell niche and promote tumor growth. *Cancer Cell* **19**, 257–272.

[5] Bergfeld SA and DeClerck YA (2010). Bone marrow–derived mesenchymal stem cells and the tumor microenvironment. *Cancer Metastasis Rev* **29**, 249–261.

[6] Karnoub AE, Dash AB, Vo AP, Sullivan A, Brooks MW, Bell GW, Richardson AL, Polyak K, Tubo R, and Weinberg RA (2007). Mesenchymal stem cells within tumour stroma promote breast cancer metastasis. *Nature* **449**, 557–563.

[7] Lecomte J, Masset A, Blacher S, Maertens L, Gothot A, Delgaudine M, Bruyere F, Carnet O, Paupert J, and Illemann M, et al (2012). Bone marrow–derived myofibroblasts are the providers of pro-invasive matrix metalloproteinase 13 in primary tumor. *Neoplasia* **14**, 943–951.

[8] Kidd S, Spaeth E, Dembinski JL, Dietrich M, Watson K, Klopp A, Battula VL, Weil M, Andreeff M, and Marini FC (2009). Direct evidence of mesenchymal stem cell tropism for tumor and wounding microenvironments using in vivo bioluminescent imaging. *Stem Cells* **27**, 2614–2623.

[9] Bernardo ME, Locatelli F, and Fibbe WE (2009). Mesenchymal stromal cells. *Ann N Y Acad Sci* **1176**, 101–117.

[10] Mi Z, Bhattacharya SD, Kim VM, Guo H, Talbot LJ, and Kuo PC (2011). Osteopontin promotes CCL5-mesenchymal stromal cell-mediated breast cancer metastasis. *Carcinogenesis* **32**, 477–487.

[11] Suzuki K, Sun R, Origuchi M, Kanehira M, Takahata T, Itoh J, Umezawa A, Kijima H, Fukuda S, and Saijo Y (2011). Mesenchymal stromal cells promote tumor growth through the enhancement of neovascularization. *Mol Med* **17**, 579–587.

[12] Spaeth EL, Dembinski JL, Sasser AK, Watson K, Klopp A, Hall B, Andreeff M, and Marini F (2009). Mesenchymal stem cell transition to tumor-associated fibroblasts contributes to fibrovascular network expansion and tumor progression. *PLoS One* **4**, e4992.

[13] Khakoo AY, Pati S, Anderson SA, Reid W, Elshal MF, Rovira II, Nguyen AT, Malide D, Combs CA, and Hall G, et al (2006). Human mesenchymal stem cells exert potent antitumorigenic effects in a model of Kaposi's sarcoma. *J Exp Med* **203**, 1235–1247.

[14] Lu YR, Yuan Y, Wang XJ, Wei LL, Chen YN, Cong C, Li SF, Long D, Tan WD, and Mao YQ, et al (2008). The growth inhibitory effect of mesenchymal stem cells on tumor cells in vitro and in vivo. *Cancer Biol Ther* **7**, 245–251.

[15] Djouad F, Plence P, Bony C, Tropel P, Apparailly F, Sany J, Noel D, and Jorgensen C (2003). Immunosuppressive effect of mesenchymal stem cells favors tumor growth in allogeneic animals. *Blood* **102**, 3837–3844.

[16] Djouad F, Bony C, Apparailly F, Louis-Plence P, Jorgensen C, and Noel D (2006). Earlier onset of syngeneic tumors in the presence of mesenchymal stem cells. *Transplantation* **82**, 1060–1066.

[17] El-Haibi CP and Karnoub AE (2010). Mesenchymal stem cells in the pathogenesis and therapy of breast cancer. *J Mammary Gland Biol Neoplasia* **15**, 399–409.

[18] Sternlicht MD and Sunnarborg SW (2008). The ADAM17-amphiregulin-EGFR axis in mammary development and cancer. *J Mammary Gland Biol Neoplasia* **13**, 181–194.

[19] Rose-John S (2013). ADAM17, shedding, TACE as therapeutic targets. *Pharmacol Res* **71**, 19–22.

[20] Busser B, Sancey L, Brambilla E, Coll JL, and Hurbin A (2011). The multiple roles of amphiregulin in human cancer. *Biochim Biophys Acta* **1816**, 119–131.

[21] Kenny PA (2007). TACE: a new target in epidermal growth factor receptor dependent tumors. *Differentiation* **75**, 800–808.

[22] Scheller J, Chalaris A, Garbers C, and Rose-John S (2011). ADAM17: a molecular switch to control inflammation and tissue regeneration. *Trends Immunol* **32**, 380–387.

[23] Peister A, Mellad JA, Larson BL, Hall BM, Gibson LF, and Prockop DJ (2004). Adult stem cells from bone marrow (MSCs) isolated from different strains of inbred mice vary in surface epitopes, rates of proliferation, and differentiation potential. *Blood* **103**, 1662–1668.

[24] Soille P (1999). Morphological Analysis, Principles and Application. Springer; 1999 [Vol.].

[25] Otsu K, Das S, Houser SD, Quadri SK, Bhattacharya S, and Bhattacharya J (2009). Concentration-dependent inhibition of angiogenesis by mesenchymal stem cells. *Blood* **113**, 4197–4205.

[26] Horiuchi K (2013). A brief history of tumor necrosis factor alpha–converting enzyme: an overview of ectodomain shedding. *Keio J Med* **62**, 29–36.

[27] Karp JM and Leng Teo GS (2009). Mesenchymal stem cell homing: the devil is in the details. *Cell Stem Cell* **4**, 206–216.

[28] Yagi H, Soto-Gutierrez A, Parekkadan B, Kitagawa Y, Tompkins RG, Kobayashi N, and Yarmush ML (2010). Mesenchymal stem cells: mechanisms of immunomodulation and homing. *Cell Transplant* **19**, 667–679.

[29] Ebert M, Yokoyama M, Kobrin MS, Friess H, Lopez ME, Buchler MW, Johnson GR, and Korc M (1994). Induction and expression of amphiregulin in human pancreatic cancer. *Cancer Res* **54**, 3959–3962.

[30] Kitadai Y, Yasui W, Yokozaki H, Kuniyasu H, Ayhan A, Haruma K, Kajiyama G, Johnson GR, and Tahara E (1993). Expression of amphiregulin, a novel gene of the epidermal growth factor family, in human gastric carcinomas. *Jpn J Cancer Res* **84**, 879–884.

[31] Chang MH, Ahn HK, Lee J, Jung CK, Choi YL, Park YH, Ahn JS, Park K, and Ahn MJ (2011). Clinical impact of amphiregulin expression in patients with epidermal growth factor receptor (EGFR) wild-type nonsmall cell lung cancer treated with EGFR-tyrosine kinase inhibitors. *Cancer* **117**, 143–151.

[32] Stabile LP, Rothstein ME, Keohavong P, Lenzner D, Land SR, Gaither-Davis AL, Kim KJ, Kaminski N, and Siegfried JM (2010). Targeting of both the c-Met and EGFR pathways results in additive inhibition of lung tumorigenesis in transgenic mice. *Cancers* **2**, 2153–2170.

[33] Normanno N, De Luca A, Bianco C, Strizzi L, Mancino M, Maiello MR, Carotenuto A, De Feo G, Caponigro F, and Salomon DS (2006). Epidermal growth factor receptor (EGFR) signaling in cancer. *Gene* **366**, 2–16.

[34] Dong J, Opresko LK, Dempsey PJ, Lauffenburger DA, Coffey RJ, and Wiley HS (1999). Metalloprotease-mediated ligand release regulates autocrine signaling through the epidermal growth factor receptor. *Proc Natl Acad Sci U S A* **96**, 6235–6240.

[35] Baillo A, Giroux C, and Ethier SP (2011). Knock-down of amphiregulin inhibits cellular invasion in inflammatory breast cancer. *J Cell Physiol* **226**, 2691–2701.

[36] Silvy M, Giusti C, Martin PM, and Berthois Y (2001). Differential regulation of cell proliferation and protease secretion by epidermal growth factor and amphiregulin in tumoral versus normal breast epithelial cells. *Br J Cancer* **84**, 936–945.

[37] Chung E, Cook PW, Parkos CA, Park YK, Pittelkow MR, and Coffey RJ (2005). Amphiregulin causes functional downregulation of adherens junctions in psoriasis. *J Invest Dermatol* **124**, 1134–1140.

[38] Chung E, Graves-Deal R, Franklin JL, and Coffey RJ (2005). Differential effects of amphiregulin and TGF-alpha on the morphology of MDCK cells. *Exp Cell Res* **309**, 149–160.

[39] Kondapaka SB, Fridman R, and Reddy KB (1997). Epidermal growth factor and amphiregulin up-regulate matrix metalloproteinase-9 (MMP-9) in human breast cancer cells. *Int J Cancer* **70**, 722–726.

[40] Menashi S, Serova M, Ma L, Vignot S, Mourah S, and Calvo F (2003). Regulation of extracellular matrix metalloproteinase inducer and matrix metalloproteinase expression by amphiregulin in transformed human breast epithelial cells. *Cancer Res* **63**, 7575–7580.

[41] Maquoi E, Sounni NE, Devy L, Olivier F, Frankenne F, Krell HW, Grams F, Foidart JM, and Noel A (2004). Anti-invasive, antitumoral, and antiangiogenic efficacy of a pyrimidine-2,4,6-trione derivative, an orally active and selective matrix metalloproteinases inhibitor. *Clin Cancer Res* **10**, 4038–4047.

[42] Willems SH, Tape CJ, Stanley PL, Taylor NA, Mills IG, Neal DE, McCafferty J, and Murphy G (2010). Thiol isomerases negatively regulate the cellular shedding activity of ADAM17. *Biochem J* **428**, 439–450.

[43] Killock DJ and Ivetic A (2010). The cytoplasmic domains of TNFalpha-converting enzyme (TACE/ADAM17) and L-selectin are regulated differently by p38 MAPK and PKC to promote ectodomain shedding. *Biochem J* **428**, 293–304.

[44] Horiuchi K, Le Gall S, Schulte M, Yamaguchi T, Reiss K, Murphy G, Toyama Y, Hartmann D, Saftig P, and Blobel CP (2007). Substrate selectivity of epidermal growth factor-receptor ligand sheddases and their regulation by phorbol esters and calcium influx. *Mol Biol Cell* **18**, 176–188.

[45] Le Gall SM, Maretzky T, Issuree PD, Niu XD, Reiss K, Saftig P, Khokha R, Lundell D, and Blobel CP (2010). ADAM17 is regulated by a rapid and reversible mechanism that controls access to its catalytic site. *J Cell Sci* **123**, 3913–3922.

[46] Dusterhoft S, Jung S, Hung CW, Tholey A, Sonnichsen FD, Grotzinger J, and Lorenzen I (2013). Membrane-proximal domain of a disintegrin and metalloprotease-17 represents the putative molecular switch of its shedding activity operated by protein-disulfide isomerase. *J Am Chem Soc* **135**, 5776–5781.

[47] Janes PW, Saha N, Barton WA, Kolev MV, Wimmer-Kleikamp SH, Nievergall E, Blobel CP, Himanen JP, Lackmann M, and Nikolov DB (2005). Adam meets Eph: an ADAM substrate recognition module acts as a molecular switch for ephrin cleavage in trans. *Cell* **123**, 291–304.

[48] Guzman MJ, Shao J, and Sheng H (2013). Pro-neoplastic effects of amphiregulin in colorectal carcinogenesis. *J Gastrointest Cancer* **44**, 211–221.

[49] Cekanova M, Masi T, Plummer III HK, Majidi M, Fedorocko P, and Schuller HM (2006). Pulmonary fibroblasts stimulate the proliferation of cell lines from human lung adenocarcinomas. *Anti-Cancer Drugs* **17**, 771–781.

[50] Mishra PJ, Mishra PJ, Humeniuk R, Medina DJ, Alexe G, Mesirov JP, Ganesan S, Glod JW, and Banerjee D (2008). Carcinoma-associated fibroblast-like differentiation of human mesenchymal stem cells. *Cancer Res* **68**, 4331–4339.

[51] Cho JA, Park H, Lim EH, and Lee KW (2012). Exosomes from breast cancer cells can convert adipose tissue-derived mesenchymal stem cells into myofibroblast-like cells. *Int J Oncol* **40**, 130–138.

[52] Gao MQ, Kim BG, Kang S, Choi YP, Yoon JH, and Cho NH (2013). Human breast cancer–associated fibroblasts enhance cancer cell proliferation through increased TGF-alpha cleavage by ADAM17. *Cancer Lett* **336**, 240–246.

[53] De Boeck A, Pauwels P, Hensen K, Rummens JL, Westbroek W, Hendrix A, Maynard D, Denys H, Lambein K, and Braems G, et al (2013). Bone marrow–derived mesenchymal stem cells promote colorectal cancer progression through paracrine neuregulin 1/HER3 signalling. *Gut* **62**, 550–560.